Vol. 39: 31–46, 2009
doi: 10.3354/cr00797

CLIMATE RESEARCH
Clim Res

Printed June 2009
Published online May 26, 2009

Climate change and drought: a risk assessment of crop-yield impacts

Yinpeng Li[1,2,*], Wei Ye[1], Meng Wang[1], Xiaodong Yan[2]

[1]The International Global Change Institute (IGCI), University of Waikato, Private Bag 3105, Hamilton 3240, New Zealand
[2]START TEA, The Institute of Atmospheric Physics, Chinese Academy of Sciences, Beijing 100029, China

ABSTRACT: We assessed the drought risk for world crop production under current and future climatic conditions by using an integrated approach to analyze the correlation between historical crop yield and meteorological drought. Future drought frequencies are estimated based on ensemble results from 20 general circulation model (GCM) climate change patterns and 6 emissions scenarios from SRES (Special Report on Emissions Scenarios) using a revised Palmer Drought Severity Index. The drought risk index was established by combining the effects of drought-disaster frequency, drought severity, production (yield) and extent of irrigation. Results indicate that, for most regions, the probability density functions (PDF) of the 120 drought disaster frequency projections for 2100 show quasi-normal distributions and consistently project higher drought disaster frequency (*DDF*) than that of baseline, which indicates an overall enhanced drought risk in the future climate change. Globally, the drought disaster-affected area will increase with the rising global temperature, from 15.4 to 44.00% by 2100. The average cropland drought risk index (*DRI*) doubles from 52.45 to 104.60 in 2050 projections. In 2100, the projection for the *DRI* increases to 129.40. Among the regions, Africa is ranked as the highest, with a baseline *DRI* value of 95.77 which increases to 205.46 in 2100 projections. Correspondingly, the rates of yield reduction related to drought disaster for major crops will increase significantly with future climate change, by >50% in 2050 and almost 90% in 2100 for the major crops. Adaptation measures to avoid aggravated drought-disaster risks are called for.

KEY WORDS: Drought disaster risk · Crop yields · Climate change impacts

1. INTRODUCTION

Globally, major increases in crop yields are required to meet the increasing demand for food. During the past several decades, world agricultural production has increased rapidly, although with significant variations (FAO 2000). Production increases are mainly due to technological developments, infrastructure improvement and investment increments, such as increases in fertilizer investment (Fan et al. 2002), while climate disasters are the main reason for variations in production. Drought occurrence is one of the world's most widespread climate disasters affecting agricultural production (UNDP 2004, Dilley et al. 2005, Helmer & Hilhorst 2006), and is therefore a determinant of world food security (Tubiello et al. 2007). An increase in the intensity, duration and area affected by drought has been observed over wider areas since the 1970s, particularly in the tropics and subtropics, where rising temperature and less precipitation have contributed to enhanced drought conditions. There is now higher confidence that climate change will increase drought risk in drought-prone areas (IPCC 2007b), placing additional stress on food security systems that are already under strain on food security systems in many regions (Rosegrant & Cline 2003, Ericksen 2008).

Due to the complexity in understanding crop yield formation and food systems, the assessment of climate change impacts on crop production has been focused on analyzing specific aspects including crop production modeling, field CO_2 fertilization effects on crop yields and socio-economic modeling (Ericksen 2008). Often the observed historical crop yields are different from the results from crop production models, because

*Email: yinpengl@waikato.ac.nz

it is difficult to incorporate all the relevant factors in model development, for instance, technological developments and agricultural adaptation measures such as new crop varieties and increases in irrigation capacity. Similarly, observed historical crop production may differ from socio-economic model predictions because of the fluctuations caused by natural disasters that are likely to be ignored in most socio-economic models. A comprehensive assessment of climate change impacts on crop production, however, requires the explicit integration of both the natural and socio-economic components related to crop yield formation.

Recently, integrated modeling frameworks have been developed for global assessment of climate change impacts on food security. For example, the International Institute for Applied Systems Analysis (IIASA) developed a system that combines the Global Agro-Ecological Zones (GAEZ) model (Batjes et al. 1997) with various general circulation models (GCMs) to provide biophysical impact analysis of climate change, and then incorporates the IIASA-Basic Linked System (BLS) to facilitate the subsequent socio-economic analysis. This modeling framework has the advantage of providing a holistic approach that integrates multiple influencing factors. Given the uncertainties associated with climate change and the complex interrelations of factors determining the threat it poses to world food security, there is a need for more methodologies and models to be developed to provide sufficient unbiased, solid information for disaster reduction and risk management (UNDP 2004). Despite their usefulness, integrated modeling frameworks introduce additional uncertainties into the final results. Given that the robustness of the overall assessment strongly depends on the performance of the underlying models which are integrated (Schmidhuber & Tubiello 2007), there is a clear need for continued and enhanced validation efforts for these modeling frameworks.

Assessments of climate change impacts on crop production must consider uncertainties in both future climate projections and the response of crops to these changes. Climate change uncertainties are often evaluated by utilizing ensemble projections from multiple climate models, and each GCM can be run with multiple greenhouse gas (GHG) emission scenarios (IPCC 2007a). Since the probabilities of individual GCM and GHG emission scenario combinations are generally unspecified, the value of multiple climate model outputs is primarily to define the range of potential changes. Differences among models can be explained by using statistical methods such as standard deviation, consistency indices (Wang 2005) and reliability-weighted averages (Giorgi & Mearns 2002).

Few studies have thoroughly evaluated the uncertainties of crop responses to climate change. In the majority of global and regional assessments, crop responses are usually simulated using process-based models that are calibrated for individual sites and then implicitly assumed to be accurate for applying to similar environmental settings and future climate conditions (Fischer et al. 2005, Parry et al. 2005). It is very hard to analyze the uncertainties in a process-based model, not only because the sources of uncertainty are complicated, but also because the parameterization processes introduce further uncertainties (Challinor et al. 2009).

Another climate change impact assessment method is to use historical crop yield data directly by quantifying the sensitivity of crops to observed climate data (Lobell et al. 2006). This method avoids the uncertainties of crop modeling. Despite the complexity of global grain production, Lobell & Field (2007) showed that simple measures of growing season temperatures and precipitation — spatial averages based on the locations of each crop — explained around 30% or more of year-to-year variations in global average yields for the world's 6 most widely grown crops. Furthermore, this method has the advantage of taking into account management level and infrastructure improvement in the assessment, as these factors are directly reflected in the observed crop yield data. Both production management and infrastructure are the main adaptation measures that can be applied for improving or stabilizing crop yield during adverse climatic conditions, such as drought. Therefore, these factors need to be integrated in the assessment of crop yield (Lobell & Asner 2003).

Various methods have been applied to study the relationship between climate variability and change and drought in different regions (Cole et al. 2002, Li et al. 2004, 2005, Wu et al. 2004, Zhang 2004, Lehner et al. 2006, Singh 2006, Alcamo et al. 2007, Prabhakar & Shaw 2008). A common feature of these studies is that the assessments focus mainly on the impacts of mean climate change (Alcamo et al. 2007), i.e. they have not considered the possibility of magnitude and/or frequency changes of extreme events, nor have they considered scenarios of abrupt climate or socio-economic change; yet any of these scenario variants is likely to have a significant impact on world crop production.

The present study aims to assess the impact of global drought risk on major crop production for current and future climates through an integrated approach, which includes several steps: (1) calculating drought disaster frequencies by employing a revised Palmer Drought Severity Index (PDSI); (2) establishing a drought risk index (*DRI*) which incorporates drought disaster frequencies, drought severity and levels of production, management and irrigation; (3) analyzing the relationship between historical crop yield reduction and the *DRI*; and (4) predicting the impacts of future climate change scenarios on crop yields.

2. MATERIALS AND METHODS

2.1. Revision of PDSI

The PDSI (Palmer 1965) has been successfully applied to quantify the severity of droughts across different climates (Wells et al. 2004) and has become a standard for measuring meteorological drought, particularly in the USA. It uses both precipitation and surface air temperature as input, in contrast to many other drought indices that are based on precipitation only (Keyantash & Dracup 2002). This allows the PDSI to take into account the effect of surface warming on droughts and wet spells, which makes it suitable for future climate change impact assessments.

By developing a global PDSI dataset, Dai et al. (1998, 2004) provided a detailed evaluation of the PDSI against available soil moisture and stream flow, and investigated the impact of surface warming of the latter half of the twentieth century on global drought and wet areas. Dai et al. (2004) emphasized that the PDSI is better used on annual time scales and should not be used as a measure for soil moisture content during cold seasons at high latitudes. In addition, quantitative interpretations of dryness or wetness for a given PDSI value depend on local climate conditions. For example, a PDSI value of 4 may imply floods in the central USA, but only moderate rainfall in northern Africa.

2.1.1. PDSI calculation

For a given year, 4 values relating to soil moisture were computed along with their complementary potential values for each month. They were: evapotranspiration (*ET*), recharge (*R*), runoff (*RO*), loss (*L*), potential evapotranspiration (*PE*), potential recharge (*PR*), potential runoff (*PRO*) and potential loss (*PL*). *PE* was estimated using Thornthwaite's method (Thornthwaite 1948). The calculation of these values depends heavily on the available water holding capacity (AWC) of the soil. The 4 potential values were weighted using α, β, γ and δ, based on local climates that reflect the 'Climatically appropriate for existing conditions' (CAFEC) values (Palmer 1965). In the present study, the observed baseline climate data were used for the calibration of these 4 potential coefficients. The coefficients were then used in PDSI calculation under both present climate and climate change scenarios.

The soil moisture departure (d) was calculated from the difference between actual precipitation (P) and the computed CAFEC precipitation $\hat{P}$:

$$d = P - \hat{P} = P - (\alpha_i PE + \beta_i PR + \gamma_i PRO - \delta_i PL) \quad (1)$$

Since the same d will have different meanings at different times and locations, it is difficult to make straightforward comparisons. To allow for reasonable comparisons to be made over time and space, the moisture departure was weighted with the climatic characteristic K, a refinement of Palmer's general approximation for the climate characteristic of a location for a month i, K':

$$K_i' = 1.5\log_{10}\left(\frac{\overline{PE}_i + \overline{R}_i + \overline{RO}_i}{\overline{P}_i + \overline{L}_i} + 2.8\right) + 0.5 \quad (2)$$

$$K_i' = \frac{17.67}{\sum_{j=1}^{12} \overline{D}_j K_j'} K_j' \quad (3)$$

where $\overline{D}_j$ is the average moisture departure for month j.

The value of 17.67 in Eq. (3) is an empirical constant derived from 9 different locations in 7 states of the USA (Palmer 1965). The result of multiplying the soil moisture departure, d, by K is called the soil moisture anomaly index, or the Z index, shown as:

$$Z = dK \quad (4)$$

The Z index is a measure of how wet or dry a given area is for a given month without regard to recent precipitation change trends. The PDSI value for a given month X_i is then calculated as:

$$X_i = 0.897X_{i-1} + \left(\frac{1}{3}\right)Z_i \quad (5)$$

This PDSI is then capable of representing drought conditions for different locations at different times and a value of −3 indicates an extreme dry condition. By applying the original PDSI, we found that the frequencies of extreme dry conditions were unreasonably low for arid areas, such as western China and the central Australian desert, because the moisture departure in these areas is small due to the low soil AWC and relatively small precipitation variability. The original PDSI cannot represent the true drought condition in these areas, where drought events occur frequently.

In the present study, the Z index was adjusted by a climatic mean Humid Index (*HI*) in order to improve the spatial comparability of the PDSI. The revised Z index, Z', is formulated as:

$$\begin{aligned} Z' &= Z \times \sqrt{HI} \quad \text{if} \quad Z > 0 \\ Z' &= Z / \sqrt{HI} \quad \text{if} \quad Z \le 0 \end{aligned} \quad (6)$$

HI is the ratio of precipitation to potential evapotranspiration (*P*/*PE*) (Hulme et al. 1992); it is a form of moisture index described by Thornthwaite (1948). The square root transformation was used to avoid the unreasonably large PDSI changes in extreme dry (e.g. *HI* = 0.2) or wet (e.g. *HI* = 2.5) regions. An *HI* value of

1.0 indicates that precipitation and potential water loss through evapotranspiration are equal. Values above 1.0 indicate a potential water surplus and values below 1.0 a potential water deficit. Hulme et al. (1992) developed a climatic classification, with different climate zones being identified on the basis of annual values of their *HI* values.

HI is the mean value of the entire calculation period. Thus this revision does not change the correlation between PDSI and the soil moisture anomaly calculated by the original PDSI program. As an index, the PDSI cannot be validated directly; however, its performance can be demonstrated by validating the *Z* value, which was carried out by Dai et al. (1998, 2004). The *HI* used in the present study was validated by Hume et al. (1992). Similar to the original PDSI, the revised PDSI cannot be validated directly. However, the soil moisture anomaly (*Z*) results in the original PDSI calculation have not been changed and, with the validated *HI*, we have assumed that the constructed index would reveal the spatial relationship between drought and crop yield at the global level, if such a relationships exists.

2.2. Relationship between drought risk and crop yield variability

2.2.1. Definition of *DRI*

Risk can be expressed as the product of the probability of a hazard and vulnerability (Jones & Mearns 2004). Hence, the risk of drought disaster can be defined as the combination of both the probability (frequency) of drought disaster occurrence and the degree of damage caused by drought disasters. In the present study, a *DRI* was used to reflect the potential adverse effects of drought. For a specific region or country *i*, its *DRI* was formulated as:

$$DRI_i = DDF_i \times DX_i(1-PDL_i)(1-AC_i) \quad (7)$$

where *DDF* is the drought disaster frequency, calculated as the proportion of the number of observed drought-affected years to the total number of observation years. For a given year, if there was one or more months in which the monthly PDSI was <–3 in the growing season, that year was counted as a drought-affected year. *DX* is the potential extent (or degree) of the drought. It was counted as the number of months in which PDSI was <–3 in the growing season in a year. For the northern hemisphere, the growing season was defined as May–September in temperate regions and March–November in tropical regions. The southern hemisphere has a season difference of 6 mo to the northern hemisphere. The production level (*PDL*) is the normalized value of the average yield of a specific crop for each country and has a range of 0.01 to 0.99, which reflects the production and management level for each country. Irrigation is the main measure used to cope with drought disaster. In the present study, drought adaptive (or coping) capacity (*AC*) is simply defined as, for the sown areas, the proportion of area equipped for irrigation, which also has a range of 0.01 to 0.99. Clearly, this definition is based on the assumption that there are unlimited water resources available for irrigation, which could be an over-simplified assumption for the complex water resource availability.

2.2.2. Extraction of meteorological yield

In the present study, meteorological yield (*MY*) was used to analyze the variations of crop yield over time. Firstly, to calculate *MY*, the time series of crop yield was detrended, assuming that the trend of the yield (which most likely is increasing) can be generally explained by technological progress and infrastructure improvement. Then, the residuals of the series were examined as the *MY*, which was postulated to depend mainly on the short term meteorological conditions (Wang et al. 2000). We employed the linear moving average method (Xue et al. 2003) for trend yield calculation. After testing with 3, 5, 10 and 20 yr linear moving averages, a 20 yr linear moving average of the annual actual crop yield per unit area (*AY*) was selected to calculate the crop trend yield (*TY*). Correspondingly, the *MY* can be expressed as:

$$MY_i = AY_i - TY_i \quad (8)$$

where *i* is year.

As a measure of crop yield fluctuation, *MY* reflects favorable and unfavorable climatic conditions and their impacts on crop production each year. Positive values of *MY* indicate increases in crop yield due to favorable climatic conditions, and negative values indicate a reduction in crop yield due to unfavorable climatic conditions, such as a drought. Finally, yield reduction rate (*YRR*) was determined as the ratio of reduced yield (the negative value of *MY*) to *TY*:

$$YRR = -MY_i/TY_i \text{ when } MY_i < 0 \quad (9)$$

2.3. Data sources

2.3.1. Baseline climate data

Global data on the sown area of major crops were obtained from Leff et al. (2004). Six of the 19 available crops were selected for the present study — rice, maize,

wheat, barley, sorghum and soybean — because they have the highest production and are widely sown. Only the grid cells where crop-sown area was >0.5% were analyzed. The global irrigation area proportion data for the turn of the 20th century were obtained from AQUA STAT (www.fao.org/nr/water/aquastat/irrigationmap/index10.stm). Global crop yields for the period 1961–2006 were obtained from FAOSTAT (http://faostat.fao.org/site/567/DesktopDefault.aspx?PageID=567) for >180 countries; crop yield data were used to analyze the relationship between crop *YRR* and the *DRI*. Observed land-surface monthly precipitation data for the period 1961–2006 was obtained from the National Centres for Environmental Prediction (NCEP; ftp://ftp.cpc.ncep.noaa.gov/precip/50yr/gauge/0.5deg/) at a spatial resolution of 0.5 × 0.5° latitude/longitude. Monthly time-series data of global terrestrial air temperature for the period 1961–2006 were at a spatial resolution of 0.5 × 0.5° (Legates & Willmott 1990). The observed monthly precipitation and temperature were then used as input to calculate the baseline PDSI.

2.3.2. Construction of future climate change data

The ensemble method was used to construct the future climate change scenarios to address the key uncertainties of GCM projections. The 20 GCMs from the Climate Model Inter-comparison Project (Covey et al. 2003) were used in the climate change projection ensemble. The relative temperature and precipitation change is expressed as the absolute change relative to change in global mean temperature from MAGICC/SCENGEN (Wigley 2007, T. M. L. Wigley 2007 pers. comm.). This method is called pattern scaling, and is used as a convenient solution to the scarcity of GCM experiments that have sampled the range of climate projection uncertainties, in particular uncertainties caused by different emissions scenarios. Pattern-scaling techniques have been developed to provide a low cost alternative to expensive atmosphere–ocean GCM and regional circulation model experiments, and for creating a range of climate scenarios that embrace uncertainties relating to different emissions concentrations and forcing scenarios (Lu & Hulme 2002, Mitchell 2003, IPCC-TGICA 2007).

This relative change pattern (or normalized pattern) is preferable to averaging GCM outputs because it controls for differences in climate sensitivity across models. SCENGEN uses results from experiments of a 1% compound CO_2 increase developed for the IPCC AR4 climate change patterns. The original resolution of these change patterns in SCENGEN is 2.5 × 2.5°, and was regridded to 0.5 × 0.5° by linear interpolation in the present study.

For the calculation of future climate PDSI, the normalized monthly change patterns of temperature and precipitation for each GCM for 12 mo were added to the baseline monthly temperature and precipitation as input:

$$T_1 = T_0 + \Delta T \times \Delta GMT_1 \quad (10)$$

$$P_1 = P_0 + P_0(\Delta P/100) \times \Delta GMT_1 \quad (11)$$

where T_1, T_0 and P_1, P_0 represent the future and baseline temperature and precipitation, respectively, ΔT and ΔP are the relative temperature and precipitation changes per 1°C global temperature change, respectively, and ΔGMT is the global mean temperature change in a projected future time. T_1 and P_1 were then were used to calculate PDSI of each grid cell for a 46 yr simulation.

2.3.3. Emissions scenarios

The time-series ΔGMT during the 21st century for the 6 IPCC illustrative emissions scenarios (A1B, A1F1, A1T, A2, B1 and B2) was obtained from MAGICC/SCENGEN (Wigley 2003). Each SRES emissions scenario used in the present study had high, mid and low climate sensitivities, and the mid sensitivity was selected. The 'business as usual scenario', or SRES A1, corresponds to the highest emissions associated with the highest temperature change, while SRES B1 corresponds to the lowest. SRES A2 assumes the highest projected population growth and is therefore associated with the highest food demand. The model run starts from 1990, with the global mean temperature change set to zero for all scenarios. For 2050, there are small differences for the increase in temperature among the 6 SRESs, ranging from 1.14°C (B1) to 1.67°C (A1FI). The temperature change differences increase with time; for instance, in 2100 the temperature rise was 4.11°C for the highest scenario, A1F1, while only 1.89°C for the B1 scenario.

Eight regions are defined in the analysis, as listed in Table 1.

Table 1. Regions and their coordinates used in the present study

Region	Coordinates
East Asia	15.0–55.0° N, 92–147° E
South Asia	3.0–39.0° N, 47–97° E
Southeast Asia	9.5–21.5° N, 92–126° E
North America	26.0–57.0° N, 57.0–124.0° W
Africa	33.0–5.5° S, 9.0–50.5° E
South America	47–12.5° N, 81–34.5° E
Oceania	11.0–48.0° S, 113.5–178.0° E
Europe	36.5–67.5° N, 11.0–46.5° E

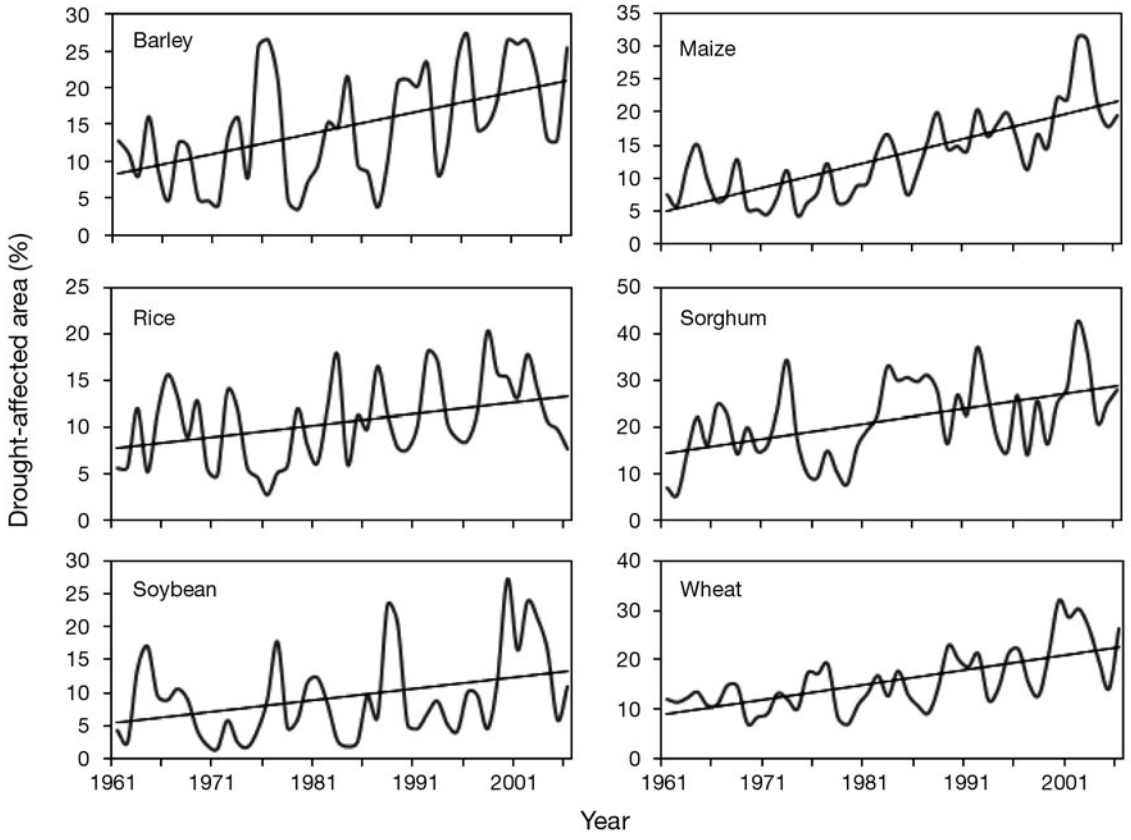

Fig. 1. Percentage of drought disaster-affected area of the major crop sown regions from 1961 to 2006. Straight lines: linear trend

3. RESULTS

3.1. Current drought risks for the sown area of global crops

Globally, since the 1960s, the sown areas for major crops have experienced a historical dry trend (Fig. 1). The drought disaster-affected areas have increased significantly since the 1970s, with a large jump in the early 1980s primarily due to precipitation decrease and subsequent expansion of surface warming in many regions (Dai et al. 1998, 2004). Overall, areas with annual occurrences of PDSI <–3 for ≥3 mo during growing season increased from 10.76% in the 1960s and 1970s to 17.10% after the 1980s (Table 2). Among the major crops, the drought-affected sown areas for maize more than doubled from 8.51 to 18.63%, and drought became more widespread for the sown areas of sorghum from 16.01 to 28.12%. The drought-affected sown areas of barley and wheat also increased significantly.

There was a dramatic increase of drought-affected areas in east and south Asia, Europe and Oceania during the late 1990s and early 2000s (Fig. 2), especially for sown areas of wheat and maize. South America and Africa were under drought conditions throughout most of the 1990s. The percentage of drought-affected areas in North America and Europe were relatively low. Africa and Oceania (mainly Australia) had very large year-to-year variability in drought-affected areas, ranging from none to almost 90%.

The spatial *DDF* pattern of crop-sown area is shown in Fig. 3. In general, the global pattern was consistent with the spatial pattern of *HI* (results not shown). Areas with *HI* > 1.0 normally had *DDF* < 0.10, mostly in

Table 2. Percentage of drought disaster-affected areas (±SD) for the major crop-sown regions during 1961–1979 and 1980–2006

	Barley	Maize	Rice	Sorghum	Soybean	Wheat	Average
1961–1979	11.23 ± 6.79	8.13 ± 3.56	8.51 ± 5.43	16.01 ± 10.04	7.31 ± 6.81	11.94 ± 3.81	10.76 ± 2.58
1980–2006	18.73 ± 7.38	18.63 ± 6.36	13.15 ± 5.18	28.12 ± 8.45	11.67 ± 8.59	20.24 ± 6.90	17.10 ± 4.48
Average	14.98 ± 7.00	13.38 ± 7.33	10.83 ± 5.97	22.07 ± 10.04	9.49 ± 7.89	16.09 ± 6.71	13.93 ± 5.44

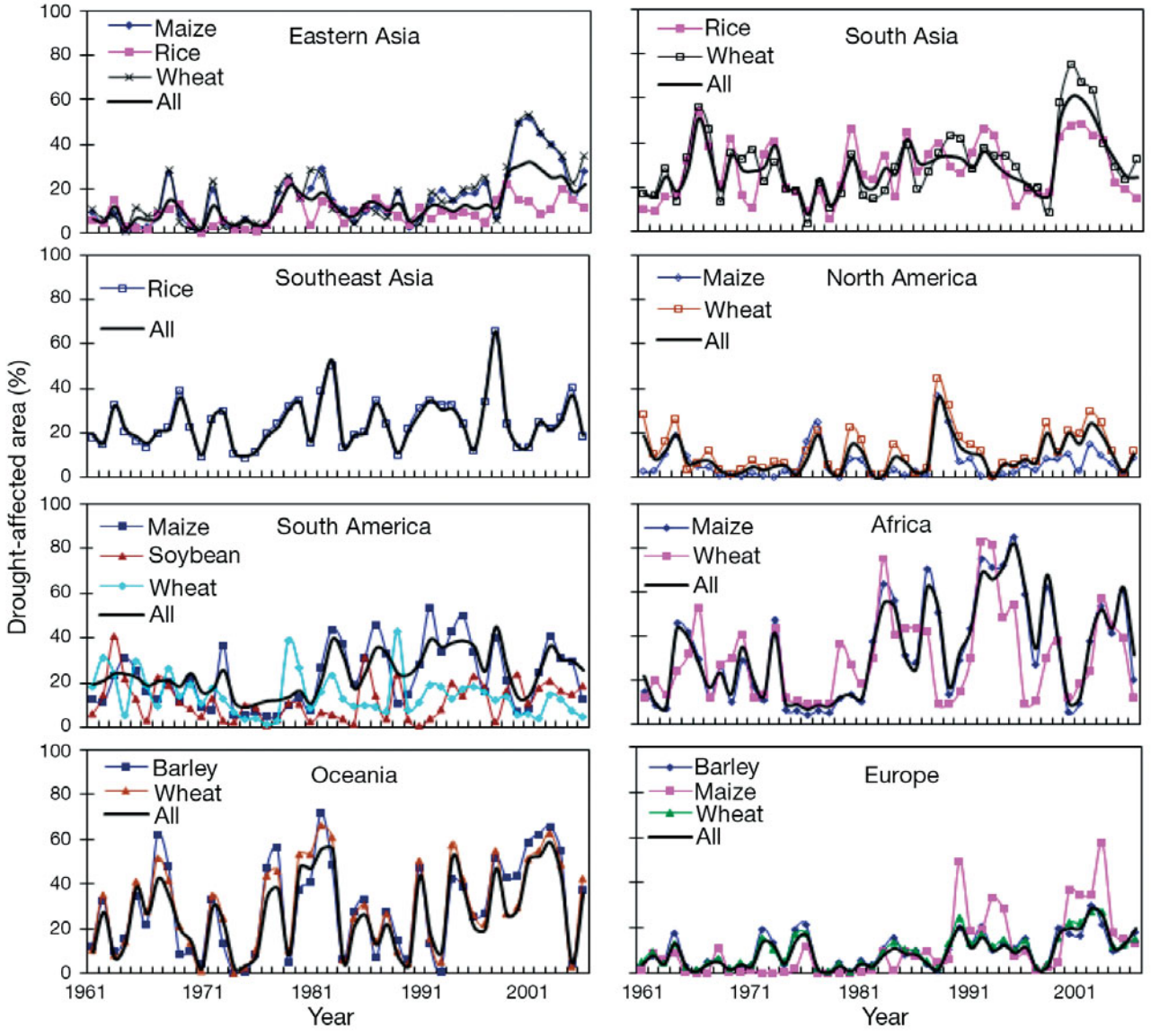

Fig. 2. Percentage of drought disaster-affected area of major cropland areas (3 mo Palmer Drought Severity Index <–3, in growing season) in different regions

humid regions; areas with *HI* = 0.5 to 0.1 normally had *DDF* = 0.1 to 0.3, mostly in semi-arid and semi-humid regions; and areas with *HI* < 0.5 normally had *DDF* > 0.3, mostly in arid regions.

3.2. GCM-projected changes to drought-affected areas and *DDF*

PDSI values were calculated by applying the GCM projected temperature and precipitation changes over the 2050 and 2100 time period. According to the statistical results, drought disaster will become more severe for most of the crop sown area, so for most of the regions drought-affected area will double (Table 3). The hotspots of future drought include southeast North America, southern China, Central America, the Mediterranean and southern Brazil, where the GCMs unanimously project higher drought disaster frequencies than under current climate conditions. For some regions, the increased drought frequencies are due to both precipitation decrease and temperature increase, such as the Mediterranean and southern Brazil, while in others the drought is primarily due to enhanced evapotranspiration due to the warming air, even when precipitation is projected to increase slightly (e.g. most areas of China) (see Fig. 3).

Despite the high degree of consistency in projecting the direction of drought changes over many regions, the 20 GCMs also produced a high standard deviation

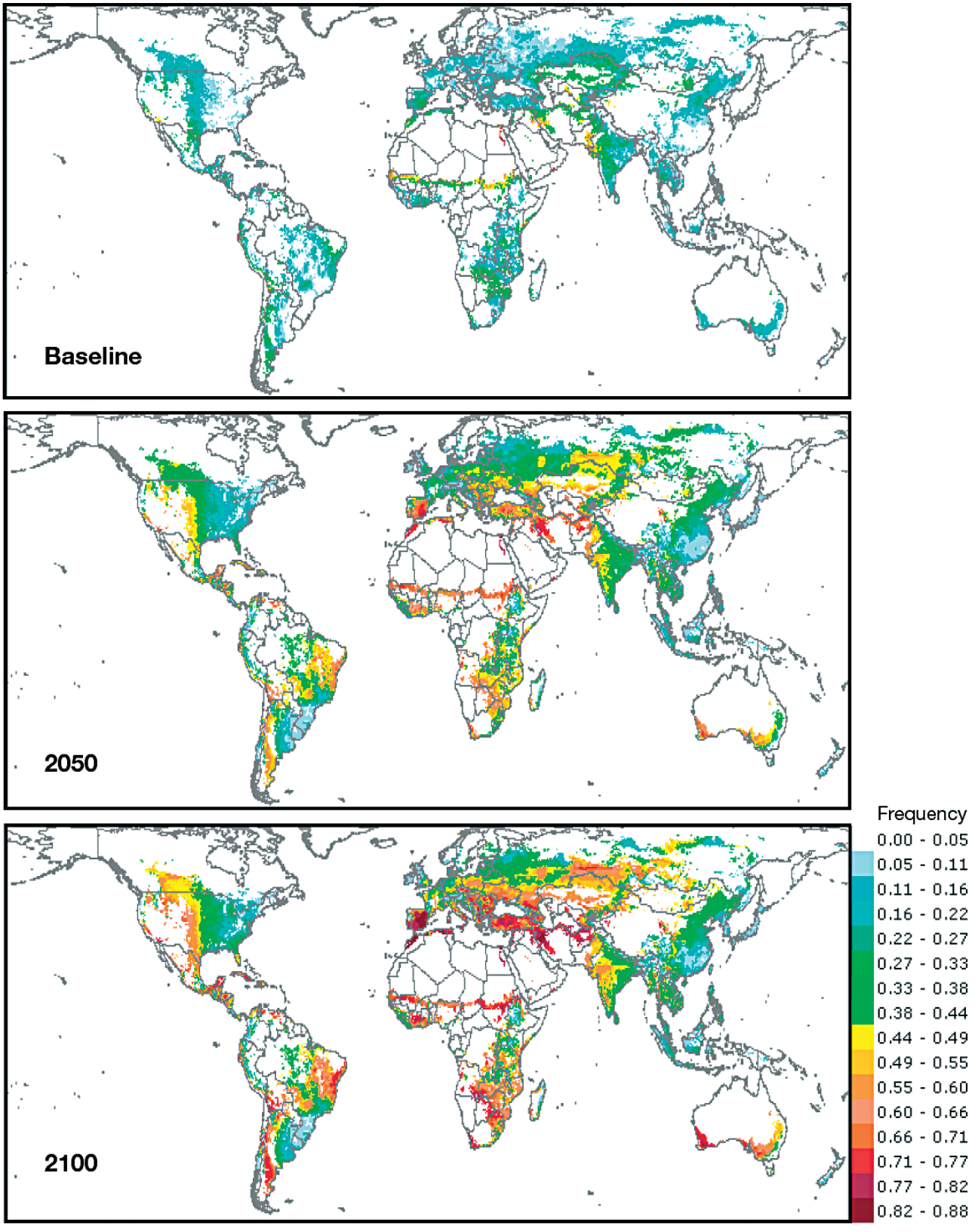

Fig. 3. Global drought disaster frequencies for the cropland growing season (3 mo Palmer Drought Severity Index <–3, in growing season) for baseline (1949–2006), 2050 and 2100 projections

Table 3. Changes in percentage of drought-affected area (±SD) for baseline and selected general circulation model (GCM) predictions

	Baseline	2100	Lowest (GCM)	Highest (GCM)
East Asia	10.41	26.97 ± 4.99	16.02 ± 2.47 (CCSM-30)	46.20 ± 7.45 (CNRM-CM)
South Asia	22.31	48.41 ± 6.56	32.48 ± 5.04 (CSIRO-30)	74.72 ± 5.43 (GISS-EH)
Southeast Asia	9.94	25.47 ± 5.93	10.11 ± 2.58 (GFDLCM21)	40.12 ± 20.63 (GISS-ER)
North America	12.02	36.71 ± 4.84	9.23 ± 4.42 (GISS-ER)	64.83 ± 7.51 (IPSL_CM)
Africa	22.01	58.80 ± 6.53	44.19 ± 4.84 (GISS-ER)	75.03 ± 6.84 (UKHADCM3)
South America	17.08	49.08 ± 7.00	36.08 ± 12.38 (GISS-ER)	61.67 ± 7.05 (IPSL_CM)
Oceania	14.89	58.54 ± 3.10	27.02 ± 5.73 (GISS-ER)	82.58 ± 3.55 (CNRM-CM)
Europe	11.13	47.26 ± 5.87	17.84 ±12.35 (GISS-ER)	67.43 ± 6.26 (UKHADCM3)
Global cropland	15.40	44.00 ± 5.78	31.31 ± 11.41 (GISS-ER)	59.47 ± 6.24 (IPSL_CM)

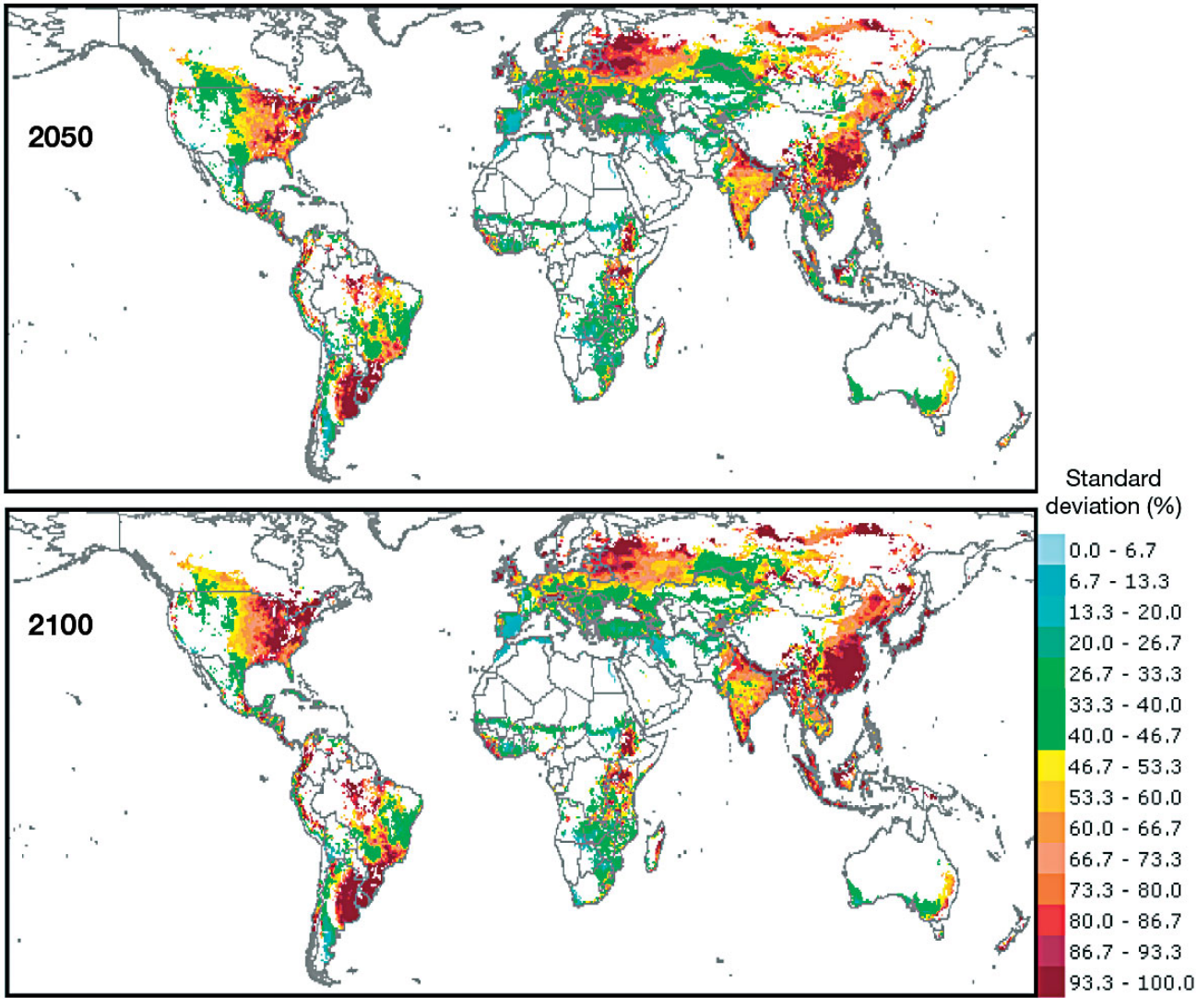

Fig. 4. Relative standard deviation (%) of drought disaster frequency change of general circulation model patterns and scenarios

in calculating the drought changes for central-eastern North America, eastern South America, southern China, Japan, North Europe and areas in eastern Africa (Fig. 4). In parts of southern China and around Uruguay the standard deviation exceeded 100%.

The global mean temperature change for 2050 and 2100 projected by the 6 SRES scenarios and the ensemble GCM patterns were used to construct future climate change scenarios, and in turn used as input to calculate the PDSI for major crop sown areas in the

world (Fig. 5). By aggregating each GCM spatial result globally, on average the *DDF*s of all major crop-sown areas become more severe than they are currently under all SRES emissions scenarios, although some GCM results show reduced *DDF*s (as indicated by the error bars in Fig. 5). In 2100, A1F1 gives the highest *DDF* value, because it has a greater temperature-increase rate than other emission scenarios, while B1 gives the lowest increase of the *DDF* value.

Spatially, the ensemble GCM projection results show a significant increase in drought-affected areas for all regions (Table 3), from 15.40 to 44.00%, by 2100. *DDF* increases in East Asia from 10.41 to 26.97% and in Southeast Asia from 9.94 to 25.47%; the 2 driest regions, South Asia and Africa, increase from 22.31 to 48.41% and 22.01 to 58.54%, respectively.

For the year 2100, the GCM GISS-ER projected the lowest drought-affected area percentages of all the GCMs and is even lower than baseline values in North America (Table 4). GFDLCM21 projected the lowest value for Southeast Asia, while CSIRO-30 and CCSM-30 projected the lowest values for South and East Asia, respectively. UKHADCM3 had the highest projections for Africa and Europe. Other GCMs which had the highest projections for different regions were CNRM-CM, IPSL_CM, GISS-EH and GISS-ER. Globally, GISS-ER had the lowest projection and IPSL_CM the highest among all GCMs.

Table 4. Drought risk index (and change, %) of different regions and future projections

	Baseline	2050	2100
East Asia	33.74	42.14 (24.90)	50.03 (48.28)
South Asia	30.34	59.95 (97.59)	71.89 (136.95)
Southeast Asia	27.73	50.81 (83.23)	67.48 (143.35)
North America	35.43	67.25 (89.81)	88.81 (150.66)
Africa	95.77	175.77 (83.53)	205.46 (114.53)
South America	41.18	98.08 (138.17)	120.68 (193.05)
Oceania	8.99	15.66 (74.19)	22.81 (153.73)
Europe	27.95	71.98 (157.53)	102.81 (267.84)
Central Asia	48.06	75.15 (56.37)	89.02 (85.23)
Middle East	45.97	85.26 (85.47)	106.24 (131.11)
Global average	52.45	104.60 (99.43)	129.24 (146.41)

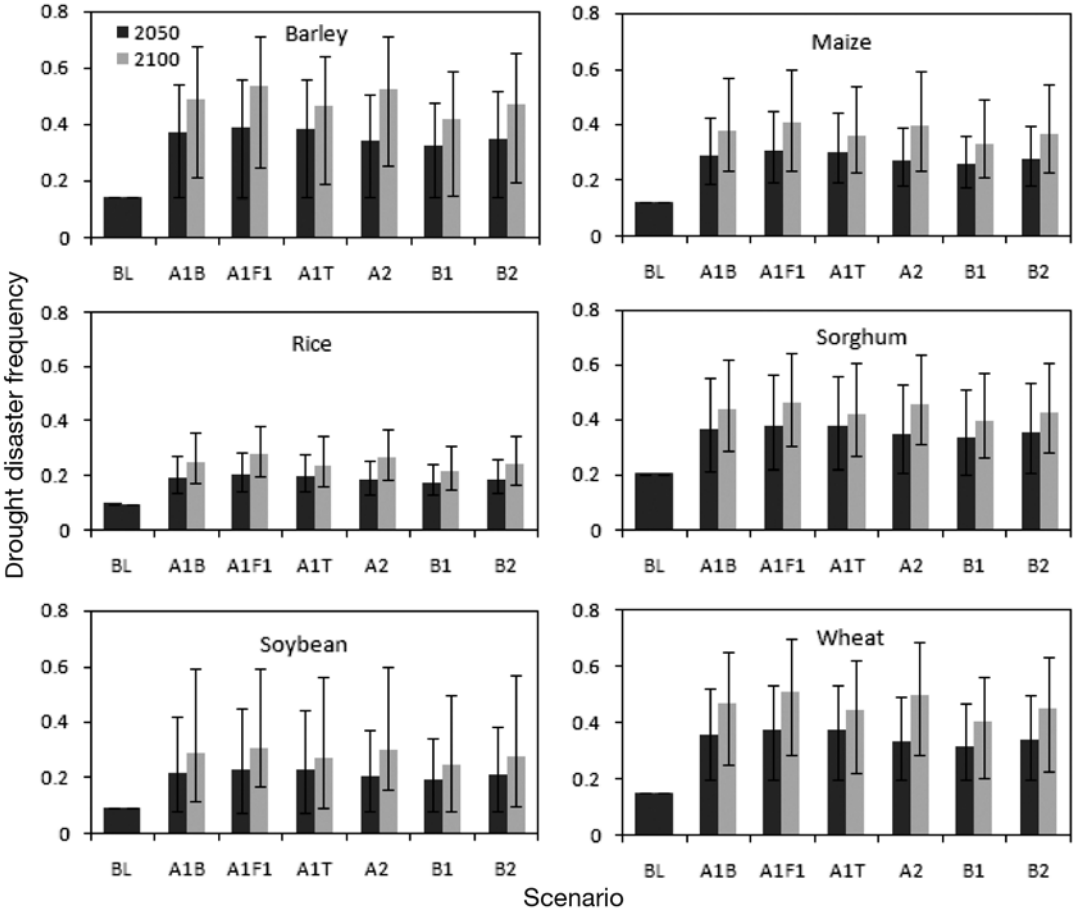

Fig. 5. Change in global drought disaster frequencies (3 mo Palmer Drought Severity Index <–3, in growing season) of major crop sown areas for 20 general circulation model (GCM) patterns and 6 SRES emissions scenarios (A1B, A1F1, A1T, A2, B1 and B2). BL: baseline. Data are average of 20 GCMs; error bars: the range of individual GCM results

3.3. Probability density distribution of future *DDF* predicted by GCMs

The standard non-parameter Gauss kernel density estimation (Parzen 1962) was employed to investigate the probability density distribution of *DDF* of the 120 projections, using 20 GCMs and 6 SRES emissions scenarios. For most regions, the probability density function (PDF) of the 120 projections for 2100 shows a quasi-normal distribution (Fig. 6). In Europe, there is a left tail on the distribution curve caused by some extreme GCM change patterns (e.g. GISS-ER). For most of the regions, the *DDF* projections of 2100 for each GCM are higher than the baseline average, which indicates an overall enhanced drought risk in the future climate change. In the *DDF* 2100 projections for Southeast and North America, there are some portions of the PDF curves lower than the baseline average line, indicating that some GCMs projected a reduced drought risk under future climate change.

3.4. Country-specific *DRI* and its relationship with crop yield reduction

A country-specific *DRI* (Eq. 7) is shown in Fig. 7. *DRI* is a synthesis of drought disaster probability, drought degree and crop land management and irrigation levels; therefore, it can be used as an indicator for yield reduction caused by meteorological drought. As shown in Fig. 7, almost all the African countries have high *DRI* values due to their arid climate, insufficient agricultural infrastructure and relatively poor management levels. Mongolia and Kazakhstan are the hotspots of drought risk in Asia, demonstrated by their high *DRI* values. South and middle Asian countries also have high *DRI*s, except those countries that have a higher percentage of irrigated cropland, e.g. Turkmenistan and Iran. The Caribbean region and parts of South America including Bolivia, Venezuela and Nicaragua have medium *DRI* values.

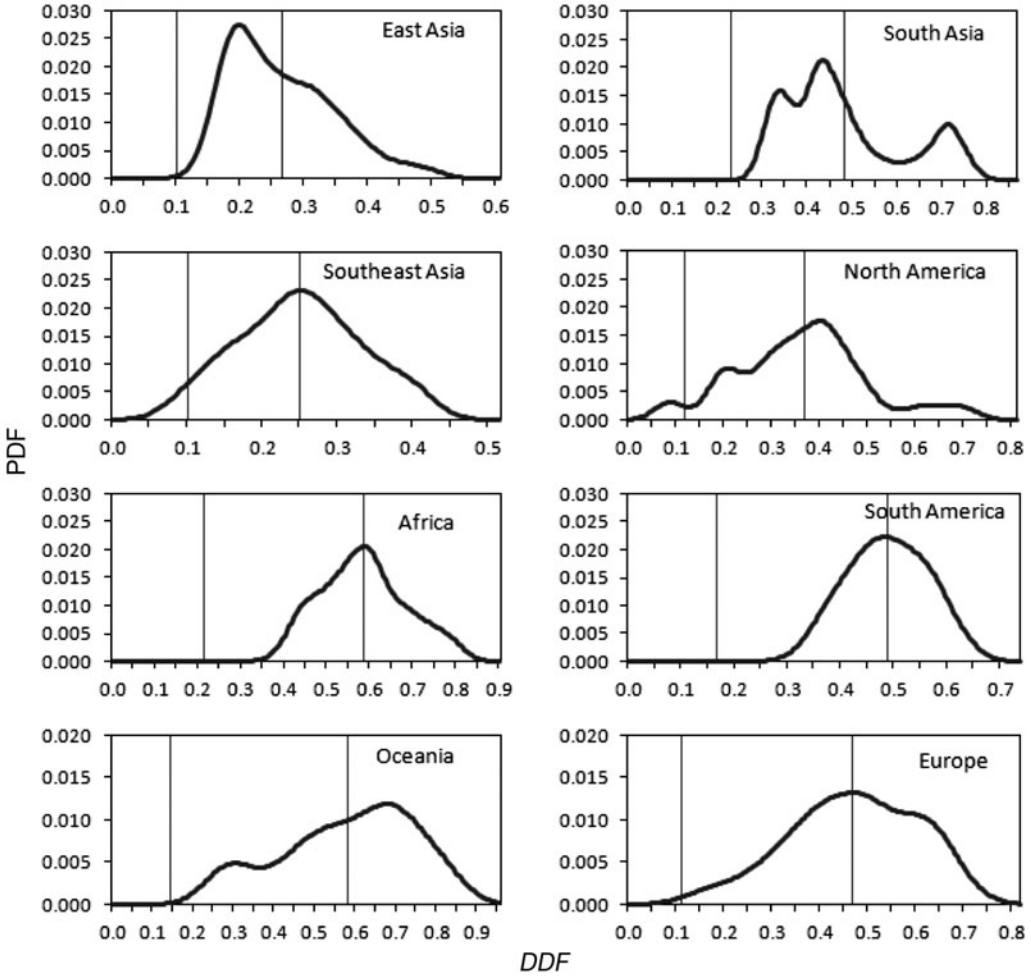

Fig. 6. Probability density function (PDF) distribution of the drought disaster frequency (*DDF*) for the different regions, predicted by 20 general circulation models and 6 SRES emissions scenarios (120 predictions in total) for 2100. The left vertical line shows the average *DDF* of the baseline; the right vertical line shows the average *DDF* in 2100 under all scenarios

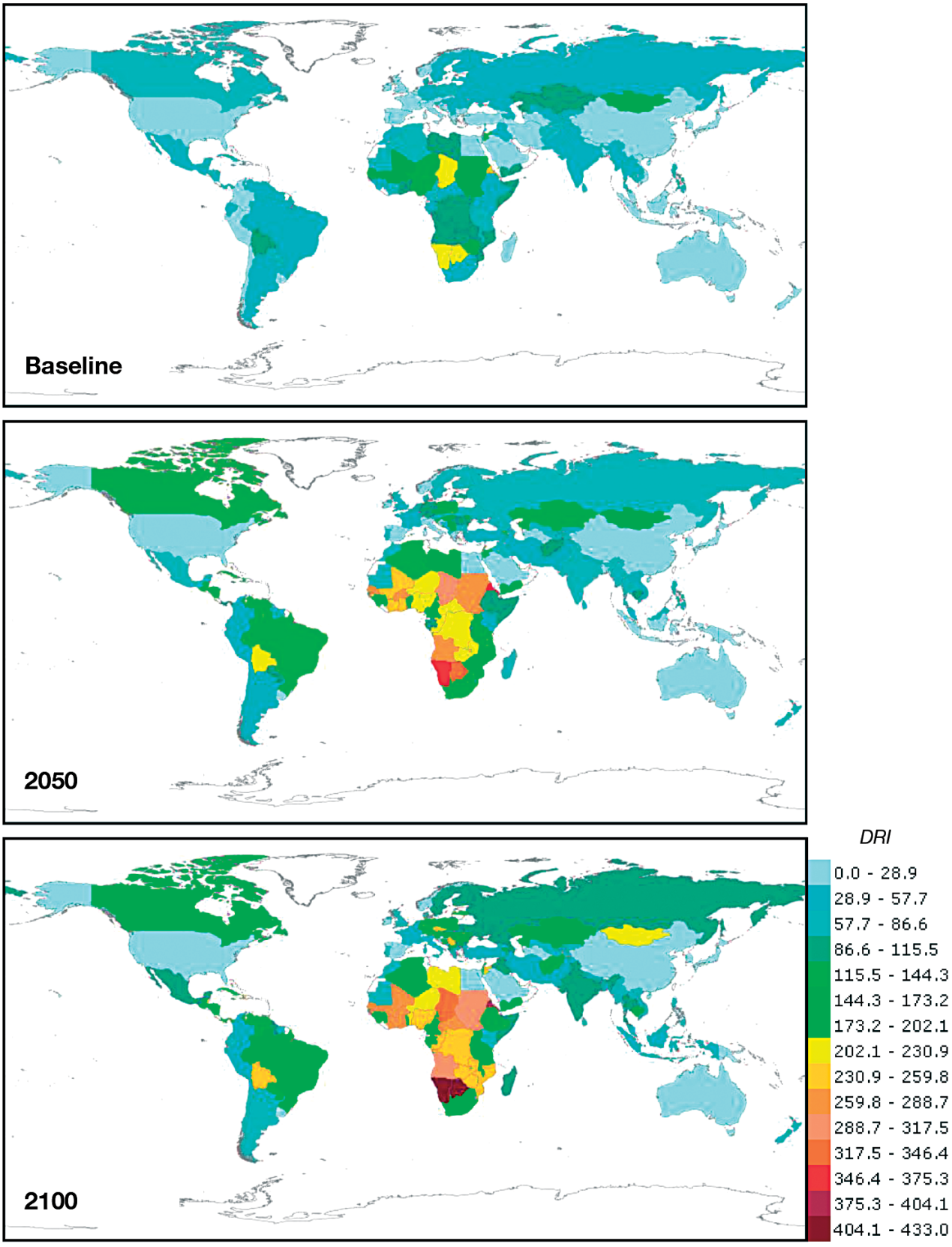

Fig. 7. Global country-specific drought risk index (*DRI*) of cropland for baseline (1961–2006), 2050 and 2100 projections

The *DRI* projections for all the regions are listed in Table 4. Globally, average cropland *DRI* doubles from 52.45 to 104.60 in 2050 projections. In 2100, the projection for the *DRI* increases to 129.40. Among the regions, Africa is ranked as the highest, with a baseline *DRI* value of 95.77 which increases to 205.46 in 2100 projections. Oceania is ranked as the lowest drought risk region, with a baseline value of 8.99, increasing to 22.81 for 2100 projections. With respect to the rate of change among the regions, Europe has the largest values: its *DRI* increases by 157.53% for 2050 and 267.84% for 2100. East Asia has the lowest rate of change values: 24.90% for 2050 and 48.28% for 2100.

The relationship between *YRR* and *DRI* of 4 major grains (barley, maize, rice and wheat) were investigated (Fig. 8) for countries that had data available; countries that have obvious distorted statistical data were omitted from the analysis. Overall, 60 to 75% of the major crop yield reductions can be explained by the *DRI*. From the established linear regression between *DRI* and *YRR*, the future *YRR* can be predicted by knowing or setting the components in *DRI*. In order to make explicit the climate change impacts, the production level and adaptive capacity are assumed to be kept constant during the future years. The changes in *DDF* and drought disaster severity and/or degree are the driving forces of *YRR*. The *YRR* of major crops from major production countries for current and future projections are summarized in Table 5. Globally, given the 2100 drought disaster condition, the *YRR* will increase from a baseline of 11.02 to 20.90% for 2100 projections for barley, from 11.98 to 26.16% for maize, from 5.82 to 9.11% for rice and from 9.59 to 18.88% for wheat. The changes for 2050 projections were also very significant for all the major crops (Table 5).

Table 5. Predicted global drought-induced yield reduction of major crops for 2050 and 2100, using the drought disaster risk index, for major production countries. *DDF*: drought disaster frequency; *DX*: potential drought extent; *DRI*: drought risk index; *YRR*: yield reduction rate

	Barley	Maize	Rice	Wheat
*DDF*_baseline	0.2193	0.2618	0.1594	0.2524
*DDF*_2050	0.3791	0.3187	0.2368	0.3767
*DDF*_2100	0.4673	0.3853	0.2876	0.4453
*DX*_baseline	0.7492	0.9183	0.5044	0.8655
*DX*_2050	1.4735	1.3075	0.9074	1.4468
*DX*_2100	1.9606	1.6781	1.1490	1.8809
*DRI*_baseline	29.25	56.43	26.37	32.53
*DRI*_2050	64.17	111.30	52.89	72.50
*DRI*_2100	83.82	140.22	67.98	95.57
*YRR*_baseline (%)	11.02	11.98	5.82	9.59
*YRR*_2050 (%)	17.35	21.26	7.84	15.48
*YRR*_2100 (%)	20.90	26.16	9.11	18.88

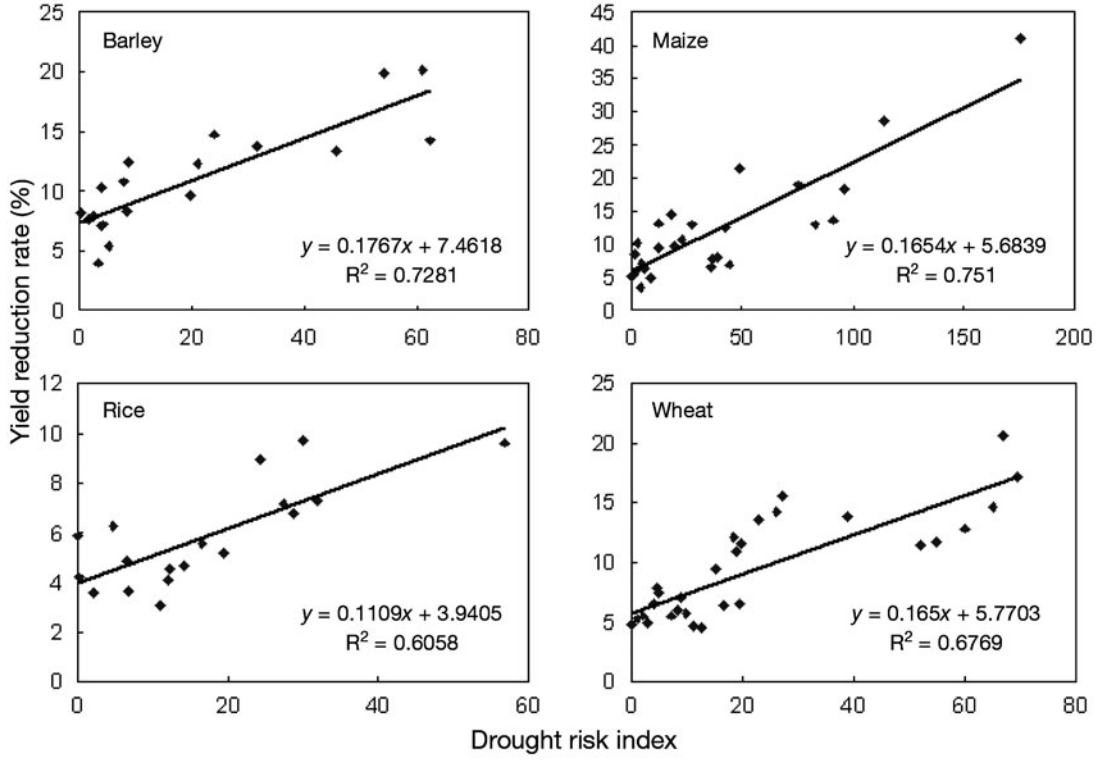

Fig. 8. Correlation between drought disaster risk index and yield reduction rate of major cropland. Dots represent different production countries. All correlation coefficients passed the 0.01 significance-level test. Note different axis scales

4. SUMMARY AND DISCUSSION

Drought is a natural phenomenon, and waxes and wanes in extent and duration in an apparently random manner. However, drought is predominantly controlled by precipitation and, to a lesser extent, by air temperature. Both of these climate variables are projected to change along with global warming, which will cause possible frequency and severity changes of drought conditions. A clear understanding of drought disaster risks to food production will enable an effective implementation of adaptive strategies to mitigate its negative effects. Drought risk to food production is considered the product of the potentially adverse effects of drought, including its frequency, intensity and severity, and the vulnerability which depends on localized socioeconomic conditions.

In the present study, natural, social and economic components were integrated for the assessment of climate change risks on drought and food production analysis. By introducing the *HI* into a revised PDSI calculation, we improved the spatial comparability of PDSI for different climate regions. The revised PDSI was used to generate global *DDF* for current and future climate conditions, and was then used in calculating the *DRI*. The relationship between world major crop yields and *DRI* was established based on specified linear regression between the historical climate data and country-specific crop yield. By validating against the current crop yield and climate conditions, the established relationship was applied to the projection of future crop yield changes under climate change scenarios. This integrated method closely links the country and regional scale drought disaster risks and their impacts on crop production based on historical data and ensemble GCM scenarios, which provide more persuasive evidence for global scale grain production risks caused by climate change.

The main finding of the present study is that by the end of the 21st century the cropland drought-disaster risk will double with rising temperature. Responding to the increase in the *DRI*, the *YRR* of major crops will increase significantly as a result of future climate change, between 34.79 to 77.51% in 2050 and 56.51 to 118.35% in 2100, varying with crop type. Globally, sorghum- and maize-sown areas are more sensitive than other crop sown areas. From the viewpoint of drought disaster *per se*, climate change-induced variation in crop production may appear as a major threat at the global scale. Regions that are already under high drought-disaster risk will be hit harder from climate change and these regions are less developed and therefore have insufficient adaptation measures. Therefore, food security assessments need to be undertaken at appropriate regional or local levels (Lobell et al. 2008)

4.1. Limitations and future research needs

In order to address the climate model uncertainties, the 20 GCM patterns listed in IPCC AR4 and 6 SRES emissions scenarios from IPCC Third Assessment Report (IPCC 2001) were used to calculate PDSI, and the ensemble results and the PDFs are presented in the present study. However, the GCM results were weighted equally. Some GCM results (e.g. GISS-ER) are very different from the majority, and therefore influence the final results. Improvement may be achieved through GCM screening and weighting, based on their performance of simulating current climate condition for different regions (Wang 2005). The present study employed the pattern scaling method for climate change projection; therefore, the climate scenarios may differ from the direct GCM outputs. Subsequently, the PDSI estimation may differ from the direct GCM output estimations carried out by other authors, such as Burke et al. (2006), although this study generally showed similar results. The differences between the pattern scaling method and direct GCM outputs needs to be further investigated (Mitchell 2003).

The present study used PDSI <–3 as the criterion for drought disaster for all regions over the world. The global spatial disaster-frequency pattern simulated with this criterion shows a reasonable fit to historical observations. However, the model performance would likely be further improved by using different PDSI criteria, or validating and adopting different PDSI for different regions. In addition, the present study only focused on the relationship between yield and drought *DRI*, which explains >60% of the yield reduction. Other affecting factors for yield reduction, including floods, pests and diseases, need to be investigated when the relevant data become available. In calculating the future *DRI*, the production level and irrigation percentage are assumed to be constant over time. However, actual production levels and irrigation percentage improve along with socioeconomic development and human adaptation. These changes are more complicated and harder to predict. Finally, the assessment was based only on current agricultural economies, over which climate changes were superimposed without readjustment of the economic conditions of countries.

4.2. Drought disaster risks and adaptations

Drought is a slow-onset natural hazard that allows for the implementation of disaster risk reduction measures. Understanding drought's evolution, complexity and social implications, including people's vulnerability to drought, will permit planners and the public

to implement effective adaptation and preparedness measures to reduce drought impacts. The present study demonstrates that, due to climate change, the trend of increasing drought risk that began at the end of the last century will continue in the 21st century. Therefore, a number of adaptation measures to combat drought disaster are called for. Adaptation refers to the change in a system in response to some force or perturbation such as climate change (Smithers & Smit 1997, Smit et al. 2000). Adaptation is not new: throughout history, people have been adapting to changing conditions. What is needed is to incorporate future climate risks into policy making (Lim & Spanger-Siegfried 2005). Adaptation also gives us an opportunity to revisit some of the unresolved disaster-reduction and sustainable-development issues. A simple way to do this is to improve the adaptive capacities in crop production systems, through such means as crop-production management and improvement of irrigation equipment, and to popularize new crop varieties. In addition, collaboration between countries experienced in drought risk reduction, and interaction with regional and international initiatives, can contribute to the development of a knowledge network to reduce the effects of drought (UN/ISDR 2007).

Acknowledgements. This study is partly supported by the Asia Pacific Network for Global Change Research (APN) CAPaBLE project, CRP2007-02CMY. Three anonymous reviewers provided substantial, valuable comments on the manuscript. Dr. L. Storey kindly proofread this manuscript.

LITERATURE CITED

Alcamo J, Droninb N, Endejana M, Golubevb G, Kirilenkoc A (2007) A new assessment of climate change impacts on food production shortfalls and water availability in Russia. Glob Environ Change 17:429–444

Batjes NH, Fischer G, Nachtergaele FO, Stolbovoi VS, van Velthuizen HT (1997) Soil data derived from WISE for use in global and regional AEZ studies. FAO/IIASA/ISRIC Report IR-97-025. International Institute for Applied Systems Analysis, Laxenburg

Burke EJ, Brown SJ, Christidis N (2006) Modeling the recent evolution of global drought and projections for the twenty-first century with the Hadley Centre climate model. J Hydrometeorol 7:1113–1125

Cole JE, Overpeck JT, Cook ER (2002) Multiyear La Niña events and persistent drought in the contiguous United States. Geophys Res Lett 29:1647 doi:10.1029/2001GL013561

Challinor AJ, Wheeler TR, Hemming D, Upadhyaya HD (2009) Ensemble yield simulations: crop and climate uncertainties, sensitivity to temperature and genotypic adaptation to climate change. Clim Res 38:117–127

Covey C, AchutaRao KM, Cubasch U, Jones P, Lambert SJ, Mann ME, Phillips TJ, Taylor KE (2003) An overview of results from the Coupled Model Intercomparison Project. Glob Planet Change 37:103–133

Dai A, Trenberth KE, Karl TR (1998) Global variations in droughts and wet spells: 1900–1995. Geophys Res Lett 25: 3367–3370

Dai A, Trenberth KE, Qian T (2004) A global data set of Palmer Drought Severity Index for 1870–2002: relationship with soil moisture and effects of surface warming. J Hydrometeorol 5:1117–1130

Dilley M, Chen RS, Deichmann U, Lerner-Lam AL, Arnold M (2005) Natural disaster hotspots: a global risk analysis. Synthesis report. International Bank for Reconstruction and Development, Washington, DC. Available at http://sedac.ciesin.columbia.edu/hazards/hotspots/synthesisreport.pdf

Ericksen PJ (2008) Conceptualizing food systems for global environmental change research. Glob Environ Change 18: 234–245

Fan S, Zhang L, Zhang X (2002) Growth, inequality, and poverty in rural China: the role of public investments. International Food Research Institute, Research Report 125, Washington, DC

FAO (2000) The state of food and agriculture 2000. II. World food and agriculture: lessons from the past 50 years. FAO, Rome

Fischer G, Shah M, Tubiello FN, van Velhuizen H (2005) Socioeconomic and climate change impacts on agriculture: an integrated assessment, 1990–2080. Philos Trans R Soc Lond B Biol Sci 360:2067–2083

Giorgi F, Mearns LO (2002) Calculation of average, uncertainty range, and reliability of regional climate changes from AOGCM simulations via the 'reliability ensemble averaging' (REA) method. J Clim 15:1141–1158

Helmer M, Hilhorst D (2006) Natural disasters and climate change. Disasters 30:1–4

Hulme M, Marsh R, Jones PD (1992) Global changes in a humidity index between 1931–60 and 1961–90. Clim Res 2:1–22

IPCC (2001) The scientific basis. Contribution of Working Group I to the Third Assessment Report of the Intergovernmental Panel on Climate Change. Cambridge University Press, Cambridge

IPCC (2007a) Summary for policymakers. In: Core Writing Team, Pachauri RK, Reisinger A (eds) Climate change 2007: synthesis report. Contribution of Working Groups I, II and III to the Fourth Assessment Report of the Intergovernmental Panel on Climate Change. IPCC, Geneva. Available at www.ipcc.ch/pdf/assessment-report/ar4/syr/ar4_syr_spm.pdf

IPCC (2007b) Summary for policymakers. In: Parry ML, Canziani OF, Palutikof JP, van der Linden PJ, Hanson CE (eds) Climate change 2007: impacts, adaptation and vulnerability. Contribution of Working Group II to the Fourth Assessment Report of the Intergovernmental Panel on Climate Change. Cambridge University Press, Cambridge, p 7–22. Available at www.ipcc.ch/pdf/assessment-report/ar4/wg2/ar4-wg2-spm.pdf

Jones R, Mearns L (2004) Assessing future climate risks. Available at www.undp.org/gef/05/documents/publications/apf%20technical%20paper05.pdf

Keyantash J, Dracup JA (2002) The quantification of drought: an evaluation of drought indices. Bull Am Meteorol Soc 83:1167–1180

Leff B, Ramankutty N, Foley JA (2004) Geographic distribution of major crops across the world. Global Biogeochem Cycles 18:GB1009 10.1029/ 2003GB002108

Legates DR, Willmot CJ (1990) Mean seasonal and spatial variability in global surface air temperature. Theor Appl Clm 41:11–21

Lehner B, Döll P, Alcamo J, Henrichs T, Kaspar F (2006) Estimating the impact of global change on flood and drought

risks in Europe: a continental, integrated analysis. Clim Change 75:273–299

Li S, Huo Z, Wang S, Liu R, Sheng S, Liu J, Ma S (2004) Risk evaluation system and models of agrometeorological disasters. J Nat Disasters 13:77–87 (In Chinese)

Li M, Li Z, Wang D, Yang X, Zhong X, Li Z, Li Y (2005) Impact of natural disasters change on grain yield in China in the past 50 years. J Nat Disasters 14:55–60 (In Chinese)

Lim B, Spanger-Siegfried E (2005) Adaptation policy frameworks for climate change: developing strategies, policies and measures. Cambridge University Press, Cambridge

Lobell DB, Asner GP (2003) Climate and management contributions to recent trends in US agricultural yields. Science 299:1032

Lobell DB, Field CB (2007) Global scale climate–crop yield relationships and the impacts of recent warming. Environ Res Lett 2:014002 doi:10.1088/1748-9326/2/1/014002

Lobell DB, Field CB, Cahill KN, Bonfils C (2006) Impact of future climate change on California perennial crop yields: model projections with climate and crop uncertainties. Agric For Meteorol 141:208–218

Lobell DB, Burke MB, Tebaldi C, Mastrandrea MD, Falcon FP, Naylor RL (2008) Prioritizing climate change adaptation needs for food security in 2030. Science 319:607 doi: 10.1126/science.1152339

Lu X, Hulme M (2002) A short note on scaling GCM climate response patterns. Prepared for the AIACC regional study teams. Available at www.aiaccproject.org/resources/GCM/ARTICLES/PATTERN_.PDF

Ma Z, Fu C (2006) Some evidence of drying trend over northern China from 1951 to 2004. Chin Sci Bull 51:2913–2925 DOI: 10.1007/ s11434-006-2159-0

Mitchell TD (2003) Pattern scaling: an examination of the accuracy of the technique for describing future climates. Clim Change 60:217–242

IPCC-TGICA (2007) General guidelines on the use of scenario data for climate impact and adaptation assessment. Version 2. Intergovernmental Panel on Climate Change, Task Group on Data and Scenario Support for Impact and Climate Assessment, IPCC, Geneva

Palmer WC (1965) Meteorological drought. US Weather Bureau Research Paper 45, Washington, DC

Parry M, Rosenzweig C, Livermore M (2005) Climate change, global food supply and risk of hunger. Philos Trans R Soc Lond B Biol Sci 360:2125–2138

Parzen E (1962) On estimation of a probability density function and mode. Ann Math Stat 33:1065–1076

Prabhakar SVRK, Shaw R (2008) Climate change adaptation implications for drought risk mitigation: a perspective for India. Clim Change 88:113–130

Rosegrant MW, Cline SA (2003) Global food security: challenges and policies. Science 302:1917–1919

Schmidhuber J, Tubiello FN (2007) Global food security under climate change. Proc Natl Acad Sci USA 104:19703–19708

Singh M (2006) Identifying and assessing drought hazard and risk in Africa. Available at http://info.worldbank.org/etools/docs/library/238222/Singh_DroughtRiskAfrica.pdf

Smit B, Burton I, Klein RJT, Wandel J (2000) An anatomy of adaptation to climate change and variability. Clim Change 45:223–251

Smithers J, Smit B (1997) Human adaptation to climatic variability and change. Glob Environ Change 7:129–146

Thornthwaite CW (1948) An approach toward a rational classification of climate. Geogr Rev 38:55–94

Tubiello FN, Soussana JF, Howden SM (2007) Climate change and food security special feature: crop and pasture response to climate change. Proc Natl Acad Sci USA 104: 19686–19690

UNDP (United Nations Development Programme) (2004) Reducing disaster risk: a challenge for development. A global report. UNDP, New York. Available at www.undp.org/cpr/whats_new/rdr_english.pdf

UN/ISDR (United Nations secretariat of the International Strategy for Disaster Reduction) (2007) Drought risk reduction framework and practices: contributing to the implementation of the Hyogo framework for action. UN/ISDR, Geneva

Wang G (2005) Agricultural drought in a future climate: results from 15 global climate models participating in the IPCC 4th assessment. Clim Dyn 25:739–753. doi:10.1007/s00382-005-0057-9

Wang S, Ye J, Qian W (2000) Predictability of drought in China. In: Wilhite DA (ed) Drought: a global assessment. Routledge, London, p 100–112

Wigley TML (2003) MAGICC/SCENGEN 4.1: Technical Manual. UCAR, Climate and Global Dynamics Division, Boulder, CO. Available at: www.cgd.ucar.edu/cas/wigley/magicc/

Willmott CJ, Matsuura K, Legates DR (2007) Global air temperature: regridded monthly and annual climatologies (Version 2.02). Available at http://climate.geog.udel.edu/~climate/html_pages/README.lw2.html

Wu H, Hubbard KG, Wilhite DA (2004) An agricultural drought risk assessment model for corn and soybeans. Int J Climatol 24:723–741 doi:10.1002/joc.1028

Xue C, Huo Z, Li S, Ye C (2003) Risk assessment of drought and yield losses of winter wheat in northern part of North China. J Nat Disasters 12:131–139

Zhang J (2004) Risk assessment of drought disaster in the maize-growing region of Songliao Plain, China. Agric Ecosyst Environ 102:133–153

Editorial responsibility: Mikhail Semenov, Harpenden, United Kingdom

Submitted: June 3, 2008; Accepted: March 10, 2009
Proofs received from author(s): May 8, 2009